Interband magnetoabsorption in strained epitaxially grown ZnTe and ZnSe

S. Lee
Department of Physics, University of Notre Dame, Notre Dame, Indiana 46556

F. Michl and U. Rössler
Institut für Theoretische Physik, Universität Regensburg, D-93040 Regensburg, Germany

M. Dobrowolska and J. K. Furdyna
Department of Physics, University of Notre Dame, Notre Dame, Indiana 46556

(Received 24 November 1997)

Interband absorption in ultrathin epilayers of ZnTe and ZnSe has been measured in magnetic fields up to 6 T with photon energies below and above the fundamental gap. The spectra clearly show the evolution of the $1s$ and $2s$ exciton states and of the rich structure arising from the formation of Landau levels in the continuum. The observed spectral features are analyzed using the 8×8 $\mathbf{k}\cdot\mathbf{p}$ model, which takes into account the residual strain introduced during sample preparation. From this analysis we extract highly accurate values for the energy gaps and the exciton binding energies. Effects of electron-hole correlation and resonant magnetopolaron coupling are also clearly detected in the continuum absorption. We discuss the dependence of these effects on Landau quantum number and the magnetic field by comparing the experimental transition energies with calculated ones. [S0163-1829(98)04316-1]

I. INTRODUCTION

In recent years, interest in wide-gap II-VI semiconductors has been steadily increasing because of the possibility of optical device applications in the short-wavelength range of the visible spectrum, where most III-V semiconductors are opaque. This has raised the demand for detailed understanding of the near-band-edge structure of these materials. The absorption edge of wide band gap II-VI semiconductors is dominated by the formation of excitons due to the electron-hole correlation. Since excitonic effects are fundamental in the interpretation of the spectra of wide-gap II-VI materials, and since they play an important role in various optoelectronic applications, it is important to determine the exciton binding energies in a direct and precise way. For bulk samples of II-VI semiconductors many photoluminescence,[1–4] reflectance,[5–7] and magnetoreflectance[8–11] experiments have already been performed on ZnTe and ZnSe in the spectral region below the band gap for the purpose of determining band parameters, such as the exciton binding energy and the effective mass. In two-photon absorption experiments,[12–15] due to their very small linewidths, it was possible to resolve and analyze polariton features and the fine structure of excited exciton states. However, none of these experiments provide *direct* spectral information on the continuum edge. Thus, in order to obtain values of exciton binding energies, theoretical models are employed that are not free of approximations and limitations. In contrast, magnetoabsorption experiments performed in the energy region below and above the fundamental gap offer the possibility of determining the energy gap with high precision, and consequently also the exciton binding energy, in a very direct way.

An externally applied magnetic field modifies the exciton states by diamagnetic shift and Zeeman splitting; a significant structure in the absorption continuum also develop as a consequence of the formation of Landau levels.[16,17] However, magneto-optical experiments are difficult to perform on the II-VI's in the region above the band gap due to very large absorption coefficients (of the order of 10^5 cm^{-1}).[18] Therefore the observation of Landau subband transitions, from which we can study the development of the band structure in a magnetic field, requires crystals which are very thin (so as to reduce continuum absorption), and of high quality (so as to make transition lines as sharp as possible). This requirement can now be met due to the development of epitaxial growth techniques such as molecular beam epitaxy.

In this paper we will describe our magnetoabsorption experiments on high quality MBE-grown ZnTe and ZnSe epilayers with photon energies below and above the fundamental gap. The characteristic spectral features[19] observed in the continuum absorption in the presence of the magnetic field $\mathbf{B}$ follow a fan chart that corresponds to transitions between hole and electron Landau levels. By extrapolating the results to $\mathbf{B}=0$, it is possible to determine directly and accurately the band edge and, consequently, also the exciton binding energy. We support the interpretation and analysis of the data by calculations of the transition energies and dipole matrix elements using a 8×8 $\mathbf{k}\cdot\mathbf{p}$ model, including the effects of strain (introduced during sample preparation) and magnetic field.[20,21] The procedure automatically establishes a complete set of band parameters for ZnSe and ZnTe. The same set of parameters also describe the diamagnetic shifts of the $1s$ and $2s$ exciton states observed in our experiment. Systematic differences between the calculated and experimental transition energies in the absorption continuum in the presence of the magnetic field also enabled us to identify the effects of Coulomb correlation[22,23] and of electron-phonon coupling.[24]

II. EXPERIMENT

The epilayer samples were grown by molecular beam epitaxy (MBE) on 500 μm thick GaAs (100) substrates. Since we expect dislocations to form at the beginning of growth to accommodate the strain due to the lattice mismatch between the epilayer and the GaAs substrate, we grow layers sufficiently thick (approximately 1.5 μm, corresponding to 2 h of growth time), in order to exceed the critical thickness required for the formation of fully relaxed materials. In this way we obtain high quality crystal material in the top region of the epitaxial layer. In order to perform optical transmission experiments it is necessary to remove GaAs substrate, which is opaque in the band gap region of ZnTe and ZnSe. For this purpose the samples were glued on glass plates, with the epilayer in contact with the glass, and the GaAs substrate exposed. The exposed GaAs substrate was then mechanically polished to a thickness of approximately 50 μm, and the remaining substrate material was etched off at room temperature with a chemical solution of NH_4OH in H_2O_2, in 1:20 ratio. Since ultrathin epilayers of highest quality are required for our transmission experiments, we also removed the dislocation-rich interface region of about 1 μm. For this purpose, the same solution as above was used for etching the ZnSe samples, while a solution consisting of CH_3OH and Br (50:1) was used for ZnTe. Since the observed excitonic transitions show a small amount of splitting between the heavy and the light hole excitons, we conclude that a residual strain must have been introduced into our samples. The strain was probably introduced either during the sample growth and not completely removed by the above preparation procedure, or it arose from a difference in the thermal expansion coefficients of the sample, the glue and the glass plate during cooling down to 1.5 K (the temperature at which the spectra were taken).

The absorption spectra showed strong Fabry-Perot interferences, which enabled us to determine the sample thickness with high precision[25] (i.e., with less than 5% uncertainty). The sample thickness d can be determined from the separations of maxima or minima in the interference pattern using the relation

$$\frac{l}{2}=2d\frac{n(\lambda)}{\lambda}-m_1, \quad l=0,1,2,\ldots, \tag{1}$$

where $n(\lambda)$ is the refractive index for wavelength λ and m_1 is the order number for the first extremum. The plot of $l/2$ versus $n(\lambda)/\lambda$ has the slope $2d$, and cuts the y axis at m_1. The experiments discussed in the next section were performed on samples with $d\approx 0.5$ μm for ZnSe and $d\approx 0.6$ μm for ZnTe.

The transmission experiments were carried out in an optical cryostat ($T\geqslant 1.5$ K) equipped with a 6-T superconducting magnet. The light source consisted of a halogen lamp and a 1-m SPEX monochromator. The slit width of the spectrometer was set to give an energy resolution of 0.3 meV. The monochromatic light was circularly polarized, so as to allow the identification of transitions between different spin states. The signal was detected by a photomultiplier tube and was sent to a lock-in amplifier and a computer-controlled analyzer for data processing and storage.

III. THEORY

A. General concept

A proper theoretical model for handling the full information of the spectra presented in Sec. IV must simultaneously account for the effect of electron-hole correlation, the complexity of the valence band structure, and the polar coupling between electrons and longitudinal optical (LO) phonons in the presence of strain and of external magnetic field. Such a complete theory does not yet exist (see reviews, Refs. 16,17). Instead, we analyze the experimental data within the following theoretical guidelines.

(1) We consider the splitting of the exciton states due to biaxial strain using the Bir-Pikus-Hamiltonian[26] (see Sec. III B).

(2) We describe the diamagnetic shift of the $1s$ and $2s$ excitons within the perturbation scheme of Refs. 27 and 28 (see Sec. IV C); i.e., we consider the terms quadratic in the γ parameter (defined as the ratio of half the cyclotron energy over the effective Rydberg constant).

(3) We calculate free-particle hole and electron Landau levels using a 8×8 $\mathbf{k}\cdot\mathbf{p}$ Hamiltonian[21] that, besides the biaxial strain, includes all terms corresponding to bilinear expressions in the components of the wave vector $\mathbf{k}$, which in the presence of a magnetic field fulfills the commutator relations according to $\mathbf{k}\times\mathbf{k}=e\mathbf{H}/i\hbar c$ (see Sec. IV C).

(4) Using the eigenstates of this 8×8 Hamiltonian, we compute the dipole matrix elements for the transitions between hole and electron Landau levels, so as to obtain the oscillator strengths for transitions in the continuum above the fundamental gap (see Secs. IV A and IV B).

(5) We take into account the effect of resonant coupling between the Landau levels and the LO phonons in order to determine the energies at which level repulsion occurs due to the resonant magnetopolaron effect[24] (see Sec. IV C).

The following parameters are involved in our analysis of the experimental data.

(1) Elastic compliance constants s_{11} and s_{12} and deformation potentials for calculating the change of the energy gap under hydrostatic deformation. Since various notations are used in this context, we quote the relation between the two common notations in use: $C_1-D_d=-(a_c-a_v)$.

(2) Deformation potential for calculating the splitting of the topmost valence band under tetragonal uniaxial or biaxial deformation ($D_u=-3b_v/2$).

(3) The fundamental energy gap E_g, which we treat as a fitting parameter.

(4) Spin-orbit-splitting of the valence band (Δ) at the center of the Brillouin zone.

(5) The effective mass m_e^* of the electrons, the Luttinger inverse mass parameters $\gamma_1,\gamma_2,\gamma_3$, effective g values of electrons g^* and holes κ,q, and Kane's matrix element P. In the 8×8 $\mathbf{k}\cdot\mathbf{p}$ model, the parameter P weights the coupling between the Γ_6 conduction band and the Γ_8 and Γ_7 valence bands. The Luttinger parameters defined in a 4×4 $\mathbf{k}\cdot\mathbf{p}$ model for the Γ_8 states must therefore be reduced by the contribution of this coupling when used in the 8×8 model. Likewise, the 2×2 block of the Γ_6 states contains the reduced values $1+2F$ of the electron mass and $g-4N_1$ of the g value derived from remote band contributions.[20]

TABLE I. Strain parameters used in the calculations.

	$s_{11}(\mathrm{Mbar}^{-1})$	$s_{12}(\mathrm{Mbar}^{-1})$	C_1-D_d(eV)	D_u(eV)
ZnTe	2.334[a]	−0.851[a]	−5.47[b]	1.875[b]
ZnSe	2.257[a]	−0.849[a]	−4.9[c]	1.725[c]

[a]Refs. 18, 29, and 31.
[b]Ref. 14.
[c]Ref. 32.

We have also checked the influence of terms in the off-diagonal block between the valence and the conduction band, which are bilinear in the components of **k**. These terms, whose weighting factor B (Ref. 21) is determined from the above parameters and the energy separation to the higher p-antibonding conduction band, lead only to minor changes in the calculated energies. The general 8×8 Hamiltonian also contains k-linear terms caused by inversion asymmetry and strain terms in the off-diagonal blocks. All these terms, not mentioned under points (1)–(5), above, have been neglected in our calculation. Finally, the cyclotron energy $\hbar\omega_c^*=\hbar eB/\mu_0 c$ and the effective Rydberg constant $R_0^*=\mu_0 e^4/2\hbar^2\epsilon^2$ are defined in terms of the reduced mass $\mu_0=(\gamma_1/m_0+1/m_e^*)^{-1}$ of the electron-hole pair; ϵ is the static dielectric constant.

The input parameters for ZnSe and ZnTe used in our calculations are given in Tables I and II. This set of parameters has already proven very satisfactory in describing a number of different experiments in earlier studies.[18,29]

B. Influence of strain

In semiconductors with the zinc-blende structure the top of the valence band at the Γ point is the fourfold degenerate Γ_8 state, which corresponds to eigenstates of the angular momentum $J=3/2$. It is well known that under uniaxial or biaxial strain this degeneracy is lifted, as described by the 4×4 strain Hamiltonian:[14,26]

TABLE II. Input parameters used in the calculations.

	ZnTe[a]	ZnSe[a]
Δ (eV)	0.970	0.403
P (meV Å)	9.964	10.628
m_e^*/m_0	0.122	0.145
g^*	−0.40	1.06
$1+2F$	−1.64	−3.83
$g-4N1$	−1.69	−1.94
γ_1	4.05	4.30
γ_2	0.98	1.14
γ_3	1.51	1.84
κ	0.14	0.20
q	0.001	0.0
$\hbar\omega_c^*(B=10\ \mathrm{T})$	14.2 meV	13.0 meV
R_0^*	14.7 meV	14.7 meV
ϵ	8.7	9.1

[a]Refs. 18, 29, and 31.

$$H_\varepsilon=(C_1-D_d)\ \mathrm{tr}\ \varepsilon\,\mathbb{1}_{4\times4}-\frac{2}{3}D_u\left[\left(J_x^2-\frac{1}{3}J^2\right)\varepsilon_{xx}+\mathrm{c.p.}\right]-\frac{4}{3}D_u'(\{J_x,J_y\}\varepsilon_{xy}+\mathrm{c.p.}),\tag{2}$$

where the angular momentum J and its components (e.g., in the basis of the eigenstates $|J=\frac{3}{2},M=\pm\frac{3}{2},\pm\frac{1}{2}\rangle$), strain tensor components ϵ_{ij}, and deformation potentials C_1-D_d, D_u, and D_u' are all 4×4 matrices. With the choice of the hydrostatic deformation potential C_1-D_d, the eigenvalues of H_ε are given with respect to the conduction band minimum. For biaxial strain in the (x,y) plane ($\varepsilon_{xy}=0$), one obtains the eigenvalues for the strain-split topmost valence band to be[3]

$$E_{\pm3/2}=\left[2(C_1-D_d)\frac{s_{11}+2s_{12}}{s_{11}+s_{12}}+\frac{2}{3}D_u\frac{s_{11}-s_{12}}{s_{11}+s_{12}}\right]\varepsilon_{\mathrm{biax}},\tag{3}$$

$$E_{\pm1/2}=\left[2(C_1-D_d)\frac{s_{11}+2s_{12}}{s_{11}+s_{12}}-\frac{2}{3}D_u\frac{s_{11}-s_{12}}{s_{11}+s_{12}}\right]\varepsilon_{\mathrm{biax}},\tag{4}$$

where s_{ij} are the elastic compliance constants. The biaxial strain $\varepsilon_{\mathrm{biax}}$ is defined as the relative deviation of the lattice constant $a_{||}$ in the plane of the strained layer from the unstrained bulk lattice constant of the sample (i.e., of ZnSe or ZnTe)

$$\varepsilon_{\mathrm{biax}}=\frac{a_{||}-a_{\mathrm{sample}}}{a_{\mathrm{sample}}}.\tag{5}$$

As we mentioned earlier, the strain in our samples arises most probably from the difference in the thermal expansion coefficients of the epilayer, the glue, and/or the glass plate. Since these quantities and their temperature dependence are not known, $\varepsilon_{\mathrm{biax}}$ is determined from the observed shift and splitting of the exciton states, which are described by Eqs. (3) and (4). In doing this, we exploit the fact that the shift of the transition energy due to the hydrostatic part of the biaxial strain and the splitting due to the uniaxial part add with the same sign for the light hole (LH) states ($M=\pm\frac{1}{2}$), but have opposite signs and thus tend to cancel for the heavy hole (HH) states ($M=\pm\frac{3}{2}$). Thus the energy of the light-hole transition is more sensitive to strain than that of the heavy holes.

IV. RESULTS AND DISCUSSION

A. Spectra at zero magnetic field

1. ZnTe

Optical transitions observed in the band edge region of a ZnTe epilayer at 1.5 K are presented in Figs. 1 and 2. In the spectrum at zero magnetic field the strongest double peak (at 2.3789 and 2.3804 eV) corresponds to the $1s$ excitonic state, and the next doublet transition (at 2.3883 and 2.3900 eV) is the $2s$ exciton state from the two top valence bands, i.e., the heavy-hole and the light-hole band. In this sample, it is clear that the second set of doublets corresponds to the $2s$ states, since the oscillator strengths of the excitons show n^{-3}

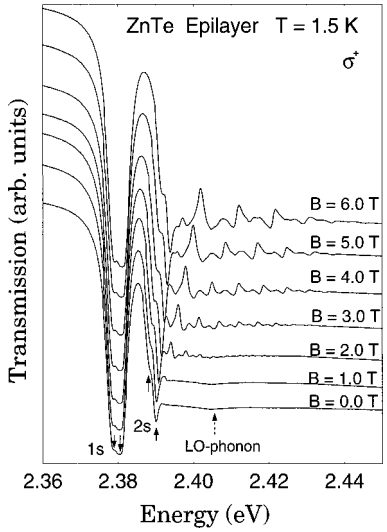

FIG. 1. Transmission spectra for ZnTe, observed at 1.5 K for σ^+ polarization in the band-edge region for several magnetic fields. The spectra show the dependence of the exciton states on magnetic field, along with the emergence of Landau level transitions in the above-band-gap continuum.

dependence.[30] The broad peak at 2.4048 eV (marked by arrow) is the LO-phonon-assisted transition: it is 25.9 meV above the 1*s* free exciton line. This value is in good agreement with the energy of LO phonons (26.1 meV), obtained from other measurements.[9] The small splitting (1.5 meV) of the exciton lines is equal to the valence band splitting [see Eqs. (3) and (4)] and can be expressed as

$$\Delta E_{1s}=E_{\pm 3/2}-E_{\pm 1/2}=\frac{4}{3}D_u\left(\frac{s_{11}-s_{12}}{s_{11}+s_{12}}\right)\varepsilon_{\text{biax}}. \qquad (6)$$

Using the observed splitting of 1.5 meV and the parameters in Table I, we obtain for the absolute value of the strain $|\varepsilon_{\text{biax}}|=0.28\times10^{-3}$. The mean value of the observed 1*s* exciton energies in our strained samples is redshifted by 1.25 meV with respect to the transverse 1*s* exciton energy of 2.3809 eV measured for unstrained bulk ZnTe.[5,14] This shift, described by the first term in Eqs. (3) and (4), leads to the conclusion that the strain is tensile, i.e., $\varepsilon_{\text{biax}}=+0.28\times10^{-3}$, which corresponds to a biaxial stress of -0.188 kbar. The calculated redshift of 1.3 meV is in accord with the above observed value of 1.25 meV.

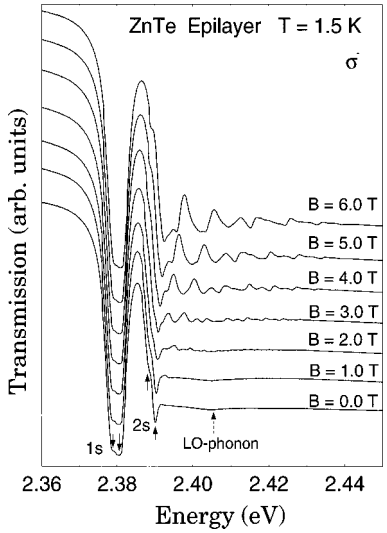

FIG. 2. Transmission spectra for ZnTe, observed at 1.5 K for σ^- polarization in the band-edge region for several magnetic fields. The spectra show the dependence of the exciton states on magnetic field, along with the emergence of Landau level transitions in the above-band-gap continuum.

In most optical experiments, transitions involving the two valence bands have different absorption intensities due to different interband dipole matrix elements M_0. Using $\mathbf{k}=0$ Bloch states, the ratio of M_0(HH) to M_0(LH) is 3, which is the squared ratio of Clebsch-Gordan coefficients for $|M|=3/2$ and $|M|=1/2$ states. However, the observed intensity of the HH exciton is not 3 times stronger than that of the LH exciton. At this point it is helpful to recall that exciton states are superpositions of pairs of electron and hole Bloch states with different $\mathbf{k}$ around the Γ point. The range of $\mathbf{k}$ values involved depends on the localization of the exciton wave function describing the relative motion of the electron-hole pair. Due to mixing at finite $\mathbf{k}$ of angular momentum states with different M, i.e., of HH and LH states, the classification of a state as HH or LH is only correct in an approximate sense, and the ratio of oscillator strengths can in practice deviate quite substantially from the value of 3 obtained for the $\mathbf{k}=0$ states. However, as is clearly seen in Figs. 1 and 2, the higher energy peak in each doublet is always stronger than the other. Since we identified the strain in this sample as tensile this can serve as qualitative support for the argument that the stronger peak should correspond to the heavy hole transition, and the weaker one should be related to the light holes.

2. ZnSe

Figures 3 and 4 show the transmission spectra observed on a ZnSe epilayer at 1.5 K. For $\mathbf{B}=0$ the exciton peaks are similar to those in the ZnTe epilayer, except for the appearance of the impurity-bound exciton at 2.7973 eV, and the absence of a clear energy splitting between the heavy and the light hole excitons in the 1*s* state. The peaks at 2.8173 and 2.8182 eV are the 2*s* states for the heavy and the light hole excitons, respectively. Since ZnSe has a larger exciton binding energy than ZnTe, it is easier to resolve higher exciton states from the onset of the continuum. For example, 3*s* states are observed in the ZnSe spectrum (2.8202 and 2.8213 eV), while they are not resolved in ZnTe. Another peak at 2.8334 eV is the LO-phonon-assisted transition, exactly 30.6 meV above the 1*s* free exciton line. Since the splitting of the 1*s* exciton line is not resolved, we took the splitting of the 2*s* exciton to calculate the value of strain in our sample. Comparing the measured splitting, $\Delta E_{2s}=0.8$ meV, with Eq. (6), and using the parameters in Table I, we obtain the magnitude of the strain as $|\varepsilon_{\text{biax}}|=0.16\times10^{-3}$. The sign of the strain is determined by comparing the center of gravity of the 1*s* exciton line with the transverse 1*s* exciton energy of unstrained ZnSe of 2.8026 eV.[15] Since the center of gravity of the strain-split excitons in our sample is blueshifted, $\varepsilon_{\text{biax}}$ must be negative (in contrast to our ZnTe sample). Thus we find a compressive strain of $\varepsilon_{\text{biax}}=-0.16\times10^{-3}$, which cor-

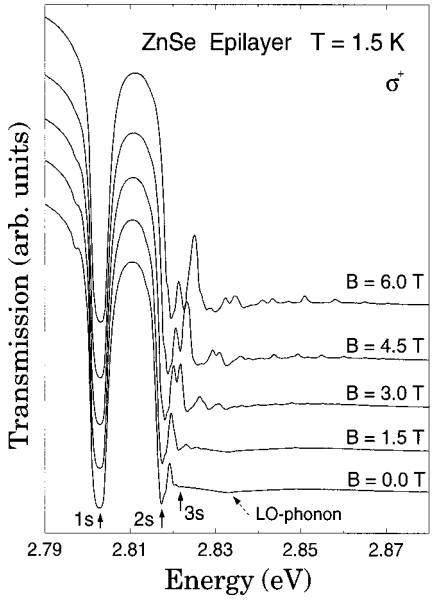

FIG. 3. Transmission spectra for ZnSe, observed at 1.5 K for σ^+ polarization in the band-edge region for several magnetic fields. The spectra show the dependence of the exciton states on magnetic field, along with the emergence of Landau level transitions in the above-band-gap continuum.

responds to a biaxial stress of $T_{\text{biax}}=0.12$ kbar. The calculated blueshift of 0.6 meV for this strain is a bit larger than the measured value of 0.4 meV. However, the difference of 0.2 meV is within our experimental resolution. The sign of the biaxial strain is also consistent with the observed intensities of the strain-split $2s$ exciton line: in contrast to ZnTe, the component with the higher intensity (identified as the HH exciton) is at lower energy than the weaker LH component. This asymmetry is not resolved in the $1s$ exciton line.

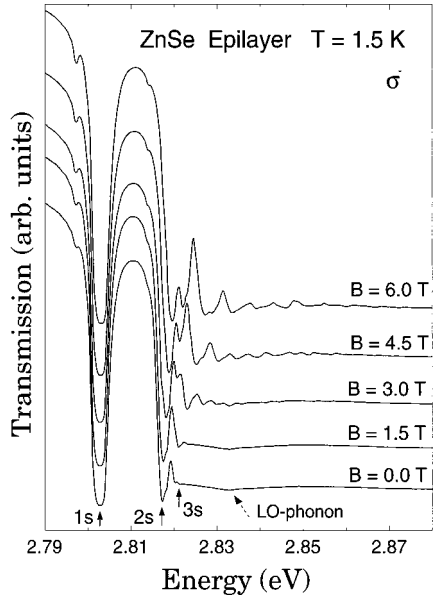

FIG. 4. Transmission spectra for ZnSe, observed at 1.5 K for σ^- polarization in the band-edge region for several magnetic fields. The spectra show the dependence of the exciton states on magnetic field, along with the emergence of Landau level transitions in the above-band-gap continuum.

B. Influence of magnetic field

Transmission spectra of the ZnTe and ZnSe epilayers become much more complex in the presence of a magnetic field, due to the combined effects of Zeeman splitting, diamagnetic shifts of excitons, and the formation of Landau levels. The progression of such exciton peaks and the emergence of the Landau level transitions as the magnetic field increases are shown for ZnTe and ZnSe in Figs. 1–4 for σ^+ and σ^- polarizations. In those figures, the low-energy parts of the spectra are dominated by exciton absorption (diamagnetic shift of hydrogenic levels), and the high-energy regions clearly show the gradual emergence of a periodic structure arising from the formation of Landau levels. We will discuss these two features below.

1. Diamagnetic shift of exciton transitions

In a magnetic field the degenerate exciton states are split into Zeeman sublevels, each sublevel experiencing a diamagnetic shift. The latter can be seen in Figs. 1,2, and 3,4 for the ZnTe and ZnSe epilayers, respectively. The diamagnetic shift is much more pronounced for the $2s$ than for the $1s$ excitons. This is depicted in Fig. 5, which shows the observed shifts of the mean value of the HH exciton energies,

$$\Delta E_{\text{dia}}=\frac{1}{2}[\Delta E(\sigma^+)+\Delta E(\sigma^-)], \tag{7}$$

plotted for $1s$ (open circles) and $2s$ (full circles) states. The change in energy ΔE is calculated with respect to the $\mathbf{B=0}$ values. The diamagnetic shift can be calculated using the expressions derived in second order perturbation theory for the low field region,[27,28] i.e., when the corrections due to the magnetic field are small compared with the binding energy of the exciton state. From Refs. 27 and 28 we have (in units of the effective Rydberg R_0^*)

$$\Delta E(1s)_{\text{dia}}=\left\{\frac{1}{2}-\left[\frac{53}{48}-\frac{53}{60}\left(\frac{3}{2}\right)^2\right]\frac{\mu_0}{\mu_1}-\frac{34}{15}\left(\frac{\mu_0}{\mu_1}\right)^2-\frac{17}{60}\left(\frac{\mu_0}{\mu_2}\right)^2\right\}\gamma^2, \tag{8}$$

$$\Delta E(2s)_{\text{dia}}=\left\{7-\left[\frac{61}{6}-\frac{122}{15}\left(\frac{3}{2}\right)^2\right]\frac{\mu_0}{\mu_1}-\frac{349}{15}\left(\frac{\mu_0}{\mu_1}\right)^2-\frac{349}{120}\left(\frac{\mu_0}{\mu_2}\right)^2\right\}\gamma^2, \tag{9}$$

where

$$\frac{m_0}{\mu_0}=\frac{m_0}{m_e^*}+\gamma_1, \quad \frac{m_0}{\mu_1}=\gamma_2, \quad \frac{m_0}{\mu_2}=2\sqrt{3}\,\gamma_3. \tag{10}$$

The γ parameter is defined as $\gamma=\hbar\omega_c^*/2R_0^*$, with $\hbar\omega_c^*=\hbar eB/\mu_0 c$ and $R_0^*=\mu_0 e^4/2\hbar^2\epsilon^2$.

The diamagnetic shifts calculated from Eqs. (8) and (9), and using the parameters of Table II, are shown in Fig. 5. For

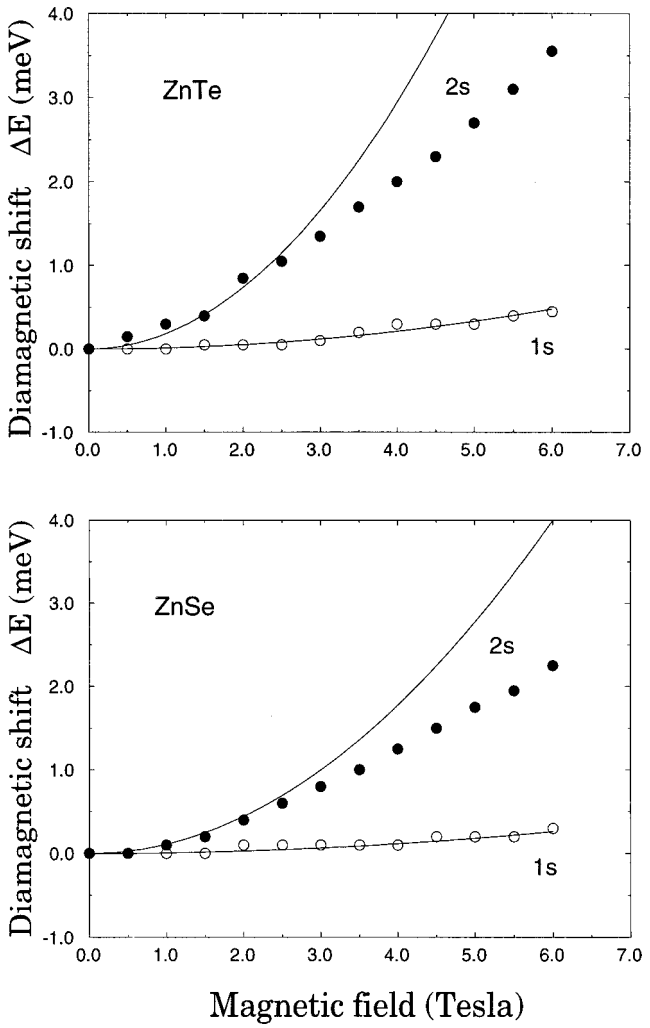

FIG. 5. Diamagnetic shifts of the $1s$ and the $2s$ excitons in ZnTe (upper panel) and in ZnSe (lower panel). Theoretical results shown by the solid lines are seen to describe rather well the $1s$ exciton data (open circles) in both materials. For $2s$ exciton, the theory agrees with experiment (solid circles) only in the low field region (smaller than 2 T), where the perturbation theory is valid.

the $1s$ excitons we find close agreement with the experimental data over the whole range of magnetic fields (up to 6 T), while for the $2s$ states the calculated shifts become too large for $B>2$ T. This is a consequence of the breakdown of the perturbation theory when the magnetic field correction is no longer small compared to the binding energy, which for the $2s$ exciton is about 4 times smaller than for the $1s$ exciton.

2. Landau level transitions

The application of a magnetic field results in a remarkable enrichment of spectroscopic details above the band gap (see Figs. 1 to 4). The new features begin to appear already at moderate magnetic fields, about 2 T, and show an oscillatory behavior with increasing intensity as the field increases. These spectral features bear the signature of Fano resonances, which result from coupling a discrete state to the continuum. In our case the discrete state is the exciton state attached to a pair of electron and hole Landau levels, while the continuum belongs to electron-hole pairs with a smaller Landau quantum number n.[19] As we mentioned before, a

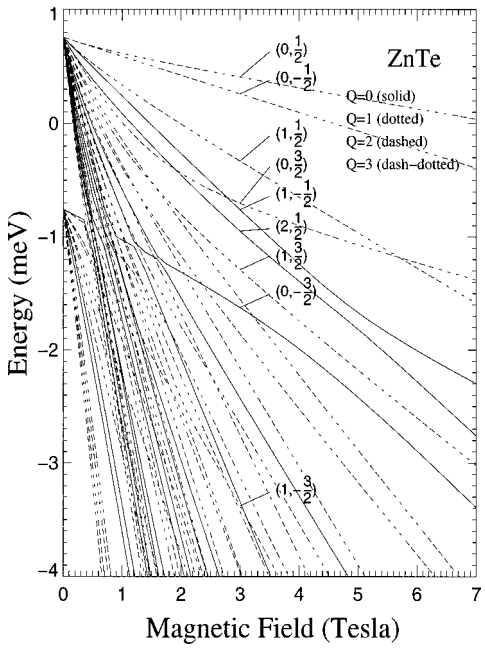

FIG. 6. Fan chart for Landau levels evolving from the strain-split valence band edge in ZnTe, calculated from the 8×8 $\mathbf{k}\cdot\mathbf{p}$ model. The levels are identified by the dominant contributing basis state at 3 T, shown in parentheses.

complete quantitative theoretical description of these transitions, taking into account electron-hole correlations in a magnetic field, is not yet available. However, if one neglects the Coulomb interaction, the behavior of an uncorrelated electron-hole pair can be described in the presence of a magnetic field by means of the developing Landau subbands. Using the 8×8 $\mathbf{k}\cdot\mathbf{p}$ model,[21] we calculated Landau level energies and dipole transition probabilities for the σ^+ and σ^- polarizations using the parameters listed in Tables I and II.

The eigenstates of the 8×8 Hamiltonian are linear combinations of products of band edge Bloch functions (characterized by a band index $\alpha=v,c$, and the z component of the spinor angular momentum M) and oscillator functions (characterized by the Landau level quantum number n)—in short notation $(n,M)_\alpha$. Such eigenstates can be identified by the dominant contributing basis state. Landau levels for the conduction band calculated from the 8×8 Hamiltonian follow a regular fan chart, with a linear dependence of the Landau level energies on **B**, and separations between the levels determined by the electron effective mass m_e^* and the g factor (Table II). This means that the nonparabolicity of the conduction band does not become visible in the relevant energy region up to about 50 meV above the band minimum. The eigenstates are strongly (to more than 95%) dominated by a single basis state $(n,M)_c$.

In contrast, the valence band Landau levels show significant deviations from this simple behavior, and a strong mixing of basis states due to the complexity of the valence band. The valence band Landau levels for ZnTe and ZnSe are plotted in Figs. 6 and 7. The levels are classified according to the fourfold symmetry corresponding to the present case (i.e., when magnetic field is applied along the [100] growth direction). The quantum number Q is explained in Ref. 21. A nonlinear dependence of the Landau levels on the magnetic

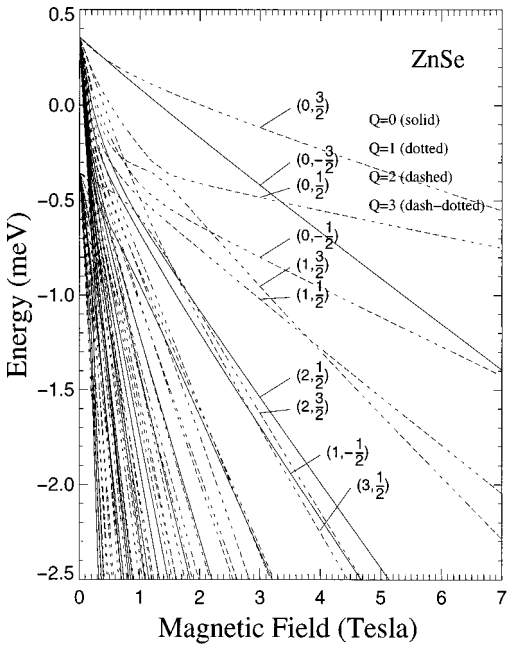

FIG. 7. Fan chart for Landau levels evolving from the strain-split valence band edge in ZnSe, calculated from the 8×8 $\mathbf{k}\cdot\mathbf{p}$ model. The levels are identified by the dominant contributing basis state at 3 T, shown in parentheses.

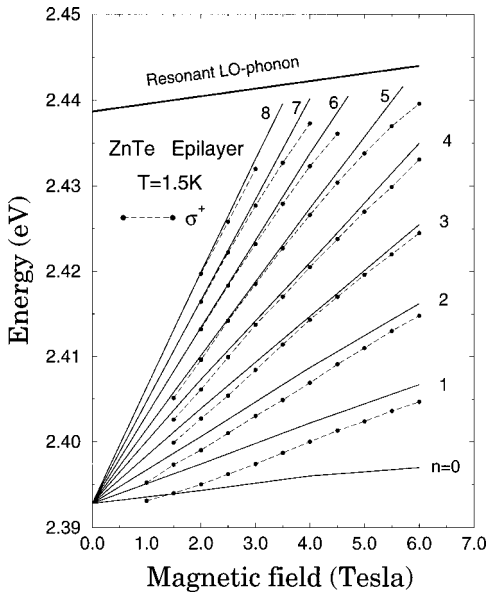

FIG. 8. Magnetic field dependence of Landau level transition energies in ZnTe for the σ^+ polarization. Experimental data are shown as points connected with dotted lines, and calculated results are given by the solid curves. The Landau quantum numbers involved in the transitions are indicated for each line. The polaron anticrossing is depicted as a thick solid line at the top of the fan chart.

field and level anticrossing are clearly seen, together with the convergence for $\mathbf{B}\rightarrow0$ to the strain-split valence band edges. In ZnSe (Fig. 7) this splitting is reversed relative to that in ZnTe (Fig. 6), in correspondence with the compressive and tensile strain, respectively. Thus, e.g., the topmost hole Landau levels are dominated by the $M=\pm3/2$ components in the former, but by the $M=\pm1/2$ components in the latter. Due to Landau level mixing, this dominance changes more rapidly for some levels with increasing magnetic field, e.g., for the fourth level in ZnTe and for the third and fourth levels in ZnSe at 3 T. Since this complex evolution of the hole Landau levels involves very small changes of energy, it cannot be resolved in the experimental spectra without a line shape analysis.

Dipole transitions from the valence to the conduction band Landau levels elicited by circularly polarized ($\sigma^{\pm}$) photons obey the selection rule $\Delta N=\pm1$, where $N=n+M+\frac{3}{2}$ is a good quantum number under axial symmetry.[21] Here n and M are the quantum numbers of the Landau oscillator and of the z component of angular momentum, respectively. Among the transitions allowed for $\Delta N=+1$, those corresponding to $(n,-\frac{3}{2})_v\rightarrow(n,-\frac{1}{2})_c$ have oscillator strengths almost a factor of 2 larger than transitions $(n,-\frac{1}{2})_v\rightarrow(n,+\frac{1}{2})_c$ or $(n,+\frac{1}{2})_v\rightarrow(n+2,-\frac{1}{2})_c$. This permits us to assign the prominent peaks in the σ^+ spectra unambiguously to $(n,-\frac{3}{2})_v\rightarrow(n,-\frac{1}{2})_c$ transitions.

After making the identification, we calculated the fan chart for the $(n,-\frac{3}{2})_v\rightarrow(n,-\frac{1}{2})_c$ transition energies, fitting them to the prominent features of the σ^+ spectra for large n ($n>5$, where we believe Coulomb correlations to be negligible). In the calculation we used parameters listed in Tables I and II, and we treated the heavy-hole energy gap as the only fitting parameter. At this point we wish to mention that the observed transition energies are very sensitive to the value of the energy gap, and therefore they provide a very direct and accurate measure of this parameter. The calculated fan chart, together with experimental points, is shown in Fig. 8 for ZnTe. The best fit was obtained for the heavy-hole band edge energy of 2.3928 ± 0.0005 eV for our strained ZnTe sample. We then found the exciton binding energy from the difference between the strain-split values of the heavy hole band edge and the HH $1s$ exciton to be

$$E_{\mathrm{ex}}=12.4\pm0.5\ \ \mathrm{meV}.$$

Taking into account corrections for the strain-induced shift and splitting of the lines, we determine the low-temperature energy gap for unstrained ZnTe to be

$$E_g=2.3934\pm0.0005\ \ \mathrm{eV}.$$

Both E_g and E_{ex} are in close agreement with values reported in the literature, as can be seen in Table III.

TABLE III. Values of fundamental energy gap E_g and of exciton binding energy at liquid helium temperature.

	E_g (eV)	Exciton binding energy (meV)	Ref.
	2.394		29
ZnTe		13.2 ± 0.3	1
	2.391		39
	2.394	12.4 ± 0.5	this paper
	2.818	21	40
ZnSe	2.8201	17.4 ± 0.4	41
		20.0	32
		20.8	42
	2.8246	22.0 ± 0.5	this paper

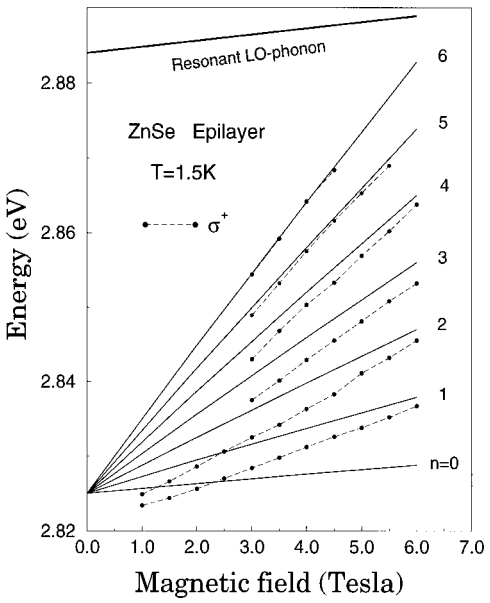

FIG. 9. Magnetic field dependence of Landau level transition energies in ZnSe for the σ^+ polarization. Experimental data are shown as points connected with dotted lines, and calculated results are given by the solid curves. The Landau quantum numbers involved in the transitions are indicated for each line. The polaron anticrossing is depicted as a thick solid line at the top of the fan chart.

We apply the same procedure to the analysis of the σ^+ spectra observed for ZnSe. The best fit to experimental data yields the HH band edge energy as 2.8250 ± 0.0005 eV (see Fig. 9). After correcting for the strain-induced shift and splitting, we find the band gap energy for unstrained ZnSe to be

$$E_g = 2.8246 \pm 0.0005 \text{ eV}.$$

We then obtain the exciton binding energy from the difference between this value and that of the $1s$ exciton energy of the unstrained material (2.8026 eV) (Ref. 15) as

$$E_{\text{ex}} = 22.0 \pm 0.5 \text{ meV}.$$

This value is somewhat bigger than the values reported in the literature, as seen in Table III, but we believe that the exciton binding energy derived from the difference between the band edge and the $1s$ exciton energy is more accurate than that determined from the $1s-2s$ exciton separation by assuming a Rydberg series. The latter assumption is not strictly correct when one considers band structure and polaron effects. Similar results as those described for the σ^+ polarization can also be obtained by analyzing the σ^- spectra of Figs. 2 and 4 which, however, have less pronounced structures than the σ^+ spectra.

One can clearly see systematic deviations of the calculated fan charts from the observed spectral positions in Figs. 8 and 9. These deviations reflect the fact that we have neglected electron-hole correlation and polar electron-phonon coupling in our calculations. We will discuss these two effects in the next section.

3. Coulomb interaction and magnetopolaron effect

Deviations of the calculated transition energies from the observed ones make it obvious that the electron-hole correlation and electron-LO phonon coupling play important roles in magneto-optical properties observed near the band gap. We start this section with a discussion of the magnetopolaron effect.

In the last few decades, a number of magneto-optical experiments have shown that the electronic energy levels in polar materials—such as CdTe, ZnTe, and ZnSe—can be significantly perturbed by the electron-LO phonon interaction. This perturbation, called the ''polaron effect,'' has been most frequently observed in cyclotron resonance experiments at low temperatures, in the form of a characteristic increase of the cyclotron mass with magnetic field.[33–37] Polaron effects can, however, also be observed in the interband magneto-optical spectra. Consider, for example, the Landau level energies in a simplified band structure:

$$\text{conduction band: } E_{\text{cn}} = E_g + \frac{1}{2}\hbar\omega_c^e + n\hbar\omega_c^e, \quad (11)$$

$$\text{valence band: } E_{\text{vn}} = \frac{1}{2}\hbar\omega_c^h + n\hbar\omega_c^h. \quad (12)$$

Electron-LO phonon interaction becomes relevant whenever the optical phonon energy is equal to an integral number of Landau level spacings, that is, $n\hbar\omega_c^e = \hbar\omega_{\text{LO}}$. Thus interband transition energies allowed by the electron-LO phonon interaction (''phonon-assisted'' transitions) are

$$\Delta E = E_{\text{cn}} - E_{\text{vn}} = E_g + \frac{1}{2}(\hbar\omega_c^e + \hbar\omega_c^h) + \hbar\omega_{\text{LO}}\left(1 + \frac{\hbar\omega_c^h}{\hbar\omega_c^e}\right), \quad (13)$$

with

$$\frac{\omega_c^h}{\omega_c^e} = \frac{m_e^*}{m_h^*}. \quad (14)$$

Thus we obtain, for single-particle transitions, a resonance with the 1-LO phonon level at

$$\Delta E = E_g + \frac{1}{2}\hbar\omega_c^0\left(\frac{m_0}{m_e} + \frac{m_0}{m_h}\right) + \hbar\omega_{\text{LO}}\left(1 + \frac{m_c^*}{m_h}\right). \quad (15)$$

The thick solid line near the top of Figs. 8 and 9 indicates the resonance with the 1-LO phonon level for transitions originating from the $(n, \pm\frac{3}{2})$ heavy hole states. In the calculations we used the Luttinger parameters from Table II to express the cyclotron masses for heavy $(+)$ and light $(-)$ holes:

$$\frac{m_h^{\pm}}{m_0} = \left[\gamma_1 \pm \left(\gamma_2^2 + \frac{3}{4}(\gamma_2 + \gamma_3)^2\right)^{1/2}\right]^{-1}. \quad (16)$$

(Note that, due to the anisotropic dispersion of the valence band, the heavy hole states, $|M| = \frac{3}{2}$, have a *smaller* cyclotron mass than the light holes.) The anticrossing of the observed transition energies with the 1-LO phonon level line due to resonant LO-phonon coupling is clearly seen for ZnTe in Fig. 8. The phenomenon strongly depends on the Landau level quantum number n. In ZnTe, about 47 meV above the

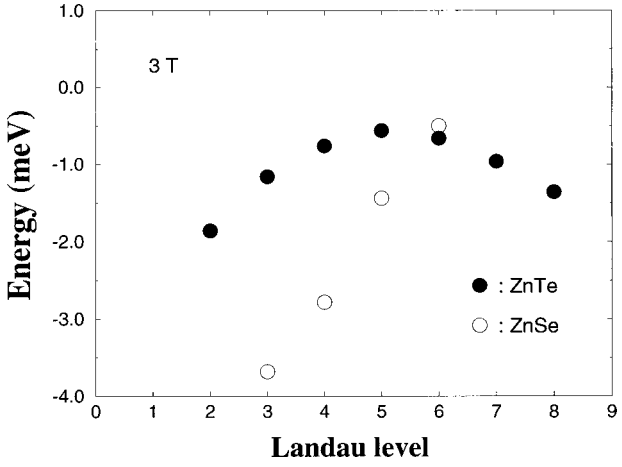

FIG. 10. Energy difference between the calculated and the experimental transition energies at $B=3$ T, as a function of Landau quantum number n. The filled and open circles represent ZnTe and ZnSe, respectively.

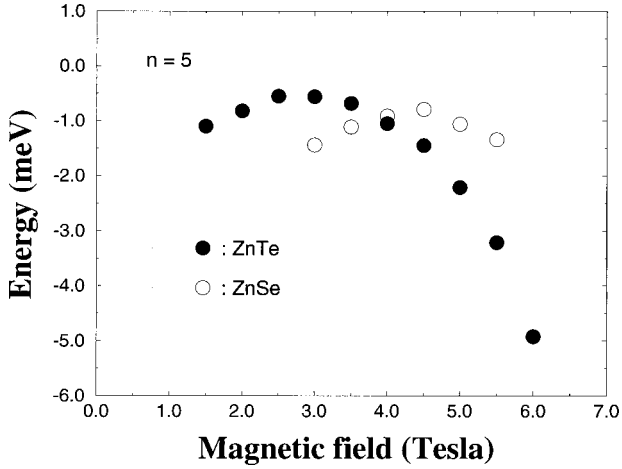

FIG. 11. Energy difference between calculated and experimental transition energies for Landau quantum number $n=5$, as a function of magnetic field **B**. The filled and open circles represent ZnTe and ZnSe, respectively.

band gap the coupling of electrons and LO phonons ($\hbar\omega_{\mathrm{LO}}=25.9$ meV) becomes pronounced, causing a broadening and damping of the absorption peaks. Thus no Landau level transitions are observed above the electron-phonon anticrossing energy. For the detected Landau level quantum numbers $n<10$ this so-called ''magnetopolaron effect'' is less pronounced for ZnSe than for ZnTe, because the LO-phonon energy is larger in ZnSe (30.6 meV), and the resonance condition is thus not fulfilled in the observed spectral range (Fig. 9). Such anticrossing, or magnetopolaron effect, has already been observed in GaAs and CdTe in earlier studies.[23,24]

In order to estimate the role of electron-hole correlation and electron-polaron coupling on interband transitions, we will compare the experimental results with calculated ones. In Fig. 10 we show the energy difference between the calculated and observed transition energies as a function of the Landau quantum number n involved in the transitions at 3 T for the σ^+ polarization, for both ZnTe and ZnSe. In the case of ZnTe, there are two regions of behavior: for lower n, where the energy difference between theoretical and experimental data shows a monotonic decrease and for higher n, where it starts to increase again. For small Landau quantum numbers (up to 4) and for low magnetic field range, the effect of the electron-phonon coupling is negligible, and the difference between the calculated and observed transition energies is only due to the Coulomb interaction, which was not taken into account in our calculations. This Coulomb correlation energy (which tends to reduce the experimental transition energy) decreases with increasing Landau quantum numbers,[38] so that the effect of the Coulomb interaction between the electrons and the holes on the Landau level transitions is stronger at lower Landau quantum numbers. For n larger than 5, we begin to observe increasing effect of the electron-phonon coupling.

In ZnSe, however, we observe only a monotonic behavior. The energy difference between theoretical and experimental data decreases continuously due to the reduction of the electron-hole correlation effect, while the magnetopolaron effect is still negligible up to Landau quantum number 6. One can observe in Fig. 10 that the discrepancies are systematically bigger in ZnSe. This indicates that electron-hole correlation effects are much more pronounced for ZnSe than for ZnTe. This should be expected, since the exciton binding energy in ZnSe is substantially larger than in ZnTe.

Figure 11 shows the energy difference between the calculated and the experimental transition energies as a function of magnetic field **B**, for the transition involving Landau quantum number $n=5$ in both ZnTe and ZnSe. This figure illustrates that the low-field region is dominated by Coulomb correlation effects, where the energy difference decreases with magnetic field and the high-field region, where the energy difference increases, is dominated by electron-phonon coupling. This behavior is characteristic for all transitions involving higher Landau quantum numbers, as can be seen from Figs. 8 and 9. The magnetic field at which experimental points are the closest to the calculated transition energies between free particle hole and electron Landau levels depends on Landau quantum number: the lower the n, the higher is the field. The reader will notice in Fig. 11 that the turning point in the difference between theory and experiment occurs at higher magnetic field in ZnSe than in ZnTe. This is because the excitonic effects are stronger in ZnSe, as mentioned before, while the polaron effects are weaker.

V. SUMMARY

In this paper we have presented magnetoabsorption data from thin MBE-grown ZnTe and ZnSe epilayers, with photon energies below and above the fundamental gap. The spectra show a rich structure due to the formation of excitons and Landau levels. We analyze these spectra in terms of available theoretical concepts, in order to determine quantitatively the fundamental energy gaps and the exciton binding energies. As these are magnetoabsorption data performed for ZnSe and ZnTe with photon energies also *above* the fundamental gap, our results are complementary to those already available in the literature. The present results confirm the reported values for gap and exciton binding energies. Furthermore, by comparing experimental results to theoretical ones, we extracted Coulomb correlation effects, which appear to be stronger when the transitions involve lower Lan-

dau levels. Another observed phenomenon which we consider to be important is the effect on the Landau level transitions of electron-phonon coupling, resulting from anticrossing between transitions and the electron-LO-phonon resonance line. Such polaron effects were observed to be stronger for the higher Landau levels and higher fields. However, the rich spectral information of the continuum absorption at finite magnetic fields cannot be fully exploited due to the absence of appropriate theoretical concepts required for interpreting the observed line shapes.

ACKNOWLEDGMENTS

This work was supported in part by the National Science Foundation Grant No. DMR 97-05064.

[1] H. Venghaus and P. J. Dean, Solid State Commun. **31**, 897 (1979).
[2] P. J. Dean, D. C. Herbert, C. J. Werkhoven, B. J. Fitzpatrick, and R. N. Bhargava, Phys. Rev. B **23**, 4888 (1981).
[3] J. Gutowski, N. Presser, and G. Kudlek, Phys. Status Solidi A **120**, 11 (1990).
[4] H. P. Wagner and H. Leiderer, in *Festkörperprobleme/Advances in Solid State Physics XXXII*, edited by U. Rössler (Vieweg, Braunschweig, 1992), p. 221.
[5] H. Leiderer, A. Supritz, M. Silberbauer, M. Lindner, W. Kuhn, H. P. Wagner, and W. Gebhardt, Semicond. Sci. Technol. **6**, A101 (1991).
[6] Y. R. Lee, A. K. Ramdas, L. A. Kolodziejski, and R. L. Gunshor, Phys. Rev. B **38**, 13 143 (1988).
[7] G. Kudlek, N. Presser, J. Gutowski, E. Abramof, and H. Sitter, Semicond. Sci. Technol. **6**, A90 (1991).
[8] H. Venghaus, P. E. Simmonds, J. Lagois, P. J. Dean, and D. Bimberg, Solid State Commun. **24**, 5 (1977).
[9] H. Venghaus, B. Jusserand, and G. Behnke, Solid State Commun. **33**, 371 (1980).
[10] S. Feierabend and H. G. Weber, Solid State Commun. **26**, 191 (1978).
[11] H. Venghaus, Solid State Commun. **26**, 199 (1978).
[12] M. Sondergeld and R. G. Stafford, Phys. Rev. Lett. **35**, 1529 (1975).
[13] M. Sondergeld, Phys. Status Solidi B **81**, 253 (1977).
[14] D. Fröhlich, F. Kubacki, M. Schlierkamp, H. Mayer, and U. Rössler, Phys. Status Solidi B **177**, 379 (1993).
[15] D. Fröhlich, W. Nieswand, U. W. Pohl, and J. Wrzesinski, Phys. Rev. B **52**, 14 652 (1995).
[16] D. Bimberg, in *Festkörperprobleme/Advances in Solid State Physics XVII*, edited by J. Treusch (Vieweg, Braunschweig, 1977), p. 195.
[17] R. P. Seisyan and B. P. Zakharchenya, in *Landau Level Spectroscopy*, edited by G. Landwehr and E. I. Rashba (Elsevier, Amsterdam, 1991), p. 347.
[18] H. Mayer, U. Rössler, and M. Ruff, Phys. Rev. B **47**, 12 929 (1993).
[19] S. Glutsch, U. Siegner, M.-A. Mycek, and D. S. Chemla, Phys. Rev. B **50**, 17 009 (1994).
[20] M. Weiler, R. L. Aggarwal, and B. Lax, Phys. Rev. B **17**, 3269 (1978).
[21] H.-R. Trebin, U. Rössler, and R. Ranvaud, Phys. Rev. B **20**, 686 (1979).
[22] W. Becker, B. Gerlach, Th. Hornung, A. Nöthe, G. Spata, and R. G. Ulbrich, in *Proceedings of the 19th International Conference on the Physics of Semiconductors* (World Scientific, Warsaw, 1988), p. 1505.
[23] A. Nöthe and G. Spata, Phys. Rev. B **39**, 8301 (1989).
[24] W. Becker, B. Gerlach, T. Hornung, and R. G. Ulbrich, in *Proceedings of the 18th International Conference on the Physics of Semiconductors* (World Scientific, Stockholm, 1986), p. 1713.
[25] B. Langen, H. Leiderer, W. Limmer, W. Gebhardt, M. Ruff, and U. Rössler, J. Cryst. Growth **101**, 718 (1990).
[26] G. E. Pikus and G. L. Bir, Sov. Phys. Solid State **1**, 1502 (1960); G. L. Bir and G. E. Pikus, *Symmetry and Strain Induced Effects in Semiconductors* (Wiley, New York, 1974).
[27] L. Świerkowski, Phys. Rev. B **10**, 3311 (1974).
[28] L. Świerkowski, Nuovo Cimento B **29**, 340 (1975).
[29] H. Mayer and U. Rössler, Solid State Commun. **87**, 81 (1993).
[30] R. J. Elliott, Phys. Rev. **108**, 1384 (1957).
[31] Landolt-Börnstein, edited by O. Madelung, New Series Group II, Vol. 22, Pt. a (Springer, Berlin, 1987).
[32] W. Gebhardt and G. Schötz, in *Properties of Wide Bandgap II-VI Semiconductors*, edited by R. Bhargava (INSPEC, The Institution of Electrical Engineers, London, 1997), p. 113.
[33] A. L. Mears, R. A. Stradling, and E. K. Inall, J. Phys. C **1**, 821 (1968).
[34] D. M. Larsen, J. Phys. C **7**, 2890 (1974).
[35] J. Waldman, D. M. Larsen, and P. E. Tannenwald, Phys. Rev. Lett. **23**, 1033 (1969).
[36] C. W. Litton, K. J. Button, J. Waldman, D. R. Cohn, and B. Lax, Phys. Rev. B **13**, 5392 (1976).
[37] Y. Imanaka, N. Miura, and H. Kukimoto, Phys. Rev. B **49**, 16 965 (1994).
[38] F. Bassani and A. Baldereschi, Surf. Sci. **37**, 304 (1973).
[39] B. Segall and D. Marple, in *Physics and Chemistry of II-VI Compounds* (North-Holland, Amsterdam, 1967), p. 319.
[40] G. E. Hite, D. T. F. Marple, M. Aven, and B. Segall, Phys. Rev. **156**, 850 (1967).
[41] H. Venghaus, Phys. Rev. B **19**, 3071 (1979).
[42] U. Neukirch, K. Wundke, J. Gutowski, and D. Hommel, Phys. Status Solidi B **196**, 473 (1996).